The International Archives of the Photogrammetry, Remote Sensing and Spatial Information Sciences, Volume XLVIII-M-6-2025
ISPRS, EARSeL & DGPF Joint Istanbul Workshop "Topographic Mapping from Space" dedicated to Dr. Karsten Jacobsen's 80th Birthday
29–31 January 2025, Istanbul, Türkiye

Investigating the New Ultracam Dragon Hybrid Aerial Mapping System

Elisa Mariarosaria Farella [1], Luca Morelli [1], Fabio Remondino [1], Rongjun Qin [2], Bernhard Schachinger [3], Klaus Legat [4]

[1] 3D Optical Metrology (3DOM) unit, Bruno Kessler Foundation (FBK), Trento, Italy - (elifarella, lmorelli, remondino)@fbk.eu
[2] Departments of Civil, Environmental and Geodetic Engineering, Electrical and Computer Engineering, Translational Data Analytics Institute, The Ohio State University, USA - qin.324@osu.edu
[3] Vexcel Imaging GmbH, Graz, Austria - bernhard.schachinger@vexcel-imaging.com
[4] AVT-Airborne Sensing Austria GmbH, Imst, Austria - k.legat@avt.at

Keywords: Hybrid Airborne System, Aerial Mapping, 3D Reconstruction, Lidar, Aerial Photogrammetry, Superpoint, Lightglue.

Abstract

Hybrid airborne systems, integrating imaging and ranging sensors within the same platform, were introduced almost ten years on the market as the new frontier of aerial mapping. Recently Vexcel Imaging developed the ULTRACAM DRAGON 4.1 hybrid airborne system which integrates a Riegl LiDAR scanner, a multi-camera imaging system and a GNSS/IMU unit. This paper investigates the characteristics and quality of derivable geospatial products, (i) examining different aerial triangulation (AT) strategies for imagery data (leveraging hand-crafted and learning-based image matching approaches for tie point extraction and (ii) evaluating the benefits of the integration of LiDAR and imaging as complementary data in supporting the 3D reconstruction of different urban environments. Moreover, the work introduces a powerful measuring tool (MEASUREE) developed by AVT-Airborne System, designed for photogrammetric analyses of large aerial blocks composed of oblique imagery.

1. Introduction

Airborne Laser Scanning (ALS) technologies (often called LiDAR) and aerial photogrammetry are consolidated and stateof-the art solutions for airborne surveying applications, including territorial mapping, monitoring and 3D city modeling (Kocaman et al., 2022). Nowadays, LiDAR and aerial photogrammetry are considered full-fledged not competing but complementary solutions, with individual benefits and opportunities for integration.

The introduction to the market first of oblique aerial systems (Cavegn et al., 2014; Remondino and Gerke, 2015; Rupnik et al., 2015; Moe et al., 2016; Remondino et al., 2016; Toschi et al., 2017a) and then of hybrid systems combining LiDAR and imaging sensors (Mandlburger et al., 2017; Toschi et al., 2018; Bacher, 2021) has opened new scenarios in the airborne mapping and geospatial fields, with the opportunity to leverage each solution's strengths while mitigating their respective limitations. If LiDAR technologies stand out for the quality and reliability of height information, rapid acquisition of large volumes of data, capacity to work in all-light and all-weather conditions, and ability to penetrate vegetation and map under dense canopy cover, photogrammetric data derived from high-resolution imagery excel for radiometric properties as well as highly detailed and faithful surface representation and image interpretation.
Existing hybrid solutions frequently embed multi-camera systems to leverage the benefit of oblique imagery in supporting and enhancing the reconstruction of complex environments (Toschi et al., 2019; Lemmens, 2020; Bacher, 2022). These systems, with a variety of possible camera configurations, number of imaging sensors and acquisition modes are especially beneficial for reconstructing occluded and narrow areas. Compared to multi-temporal data integration and fusion (Fernandez et al., 2021; Megahed et al., 2021l; Toschi et al., 2021; Norton et al., 2022), hybrid systems offer the clear advantage of concurrent data acquisition, which allows for fully exploiting the complementarity of the technologies to produce consistent mapping results. The synchronized data collection facilitates the seamless integration of different-source data by minimizing co-registration errors due to environmental changes or temporal inconsistencies.

While recent technological advancements are evident, a few studies have deepened the real benefits of these solutions for the geospatial sector (Mandlburger et al., 2017; Toschi et al., 2018). Few works have proposed new hybrid methods for simultaneously process aerial LiDAR and photogrammetric data (Glira et al., 2019; Jonassen et al., 2023; Yadav et al., 2023; Jonassen et al., 2024). Huang et al. (2018), assuming a correct data georeferencing, proposed a complementary data fusion to improve low-resolution-high-accuracy laser range data with high-resolution photogrammetric point clouds. Currently, in most of the cases, the LiDAR strip adjustment and the aerial triangulation are separate processes, and the data itegration is performed only at a later stage, limiting the potential benefits of hybrid systems in minimizing inconsistent data registration.

1.1 Paper Aims

The paper explores 3D mapping capabilities of the latest hybrid airborne systems offered by Vexcel Imaging, i.e. the ULTRACAM DRAGON 4.1. The investigation includes:

- Automated tie point extraction with hand-crafted (Section 3.1) and deep learning (Section 3.2) methods to increase connectivity between image pairs;
- Different aerial triangulation (AT) approaches (Section 3.3) for imagery data;
- Integration's quality of photogrammetric and LiDAR data (Section 3.4);
- The potential of the MEASUREE tool for photogrammetric analyses of aerial image blocks (Section 3.5).

2. The Ultracam Dragon 4.1 Hybrid System

The ULTRACAM DRAGON 4.1 (Figure 1) is the first hybrid aerial mapping technology developed by Vexcel Imaging. It integrates a Riegl VQ-680 waveform LiDAR scanner (1052 nm wavelength, up to 2 mil. measurements/second), a multi-camera imaging system for nadir and oblique acquisitions (1 RGB and 1 NIR nadir, 4 RGB oblique cameras) and an UltraNav v7 (flight management and direct georeferencing solution). For the imaging part, two focal length configurations are possible: 80 mm and 123 mm for nadir and oblique, respectively, or 50 mm and 80 mm.

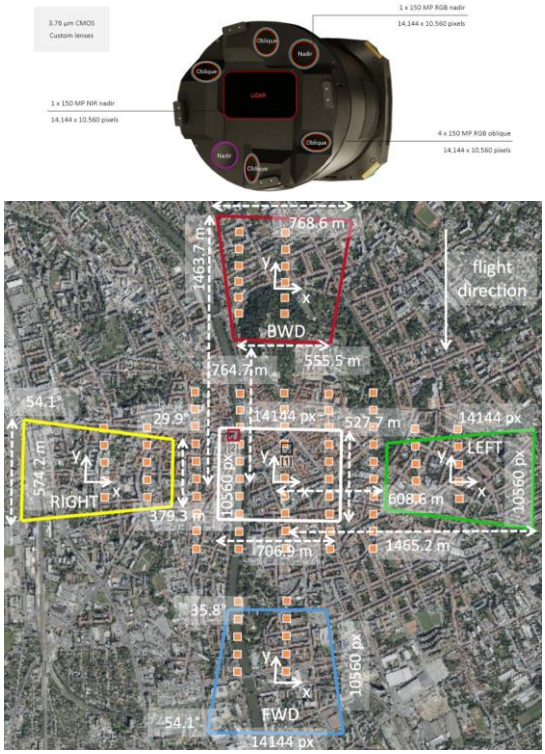

Figure 1. The ULTRACAM DRAGON 4.1 hybrid system (above). The image orientation and footprint distances in case of a flying heigh of approx. 1000 m (below).

A peculiarity of the imaging system is the shift of the sensor in the left and right cameras (portrait oriented) to optimize the image content (Figure 2).

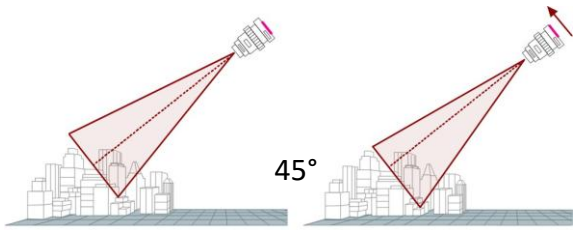

Figure 2. Effects of the (left & right) camera sensor shifting for image content optimization.

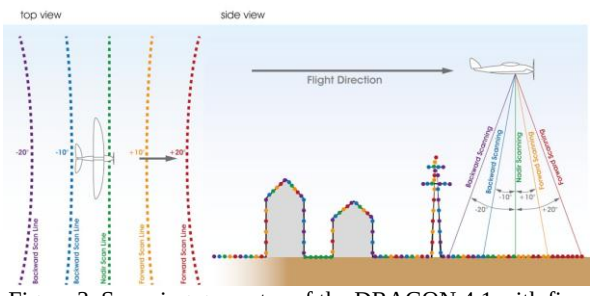

Figure 3. Scanning geometry of the DRAGON 4.1 with five scan lines and different incident angles to increase viewpoints.

The scanning mechanism has a rotating polygon mirror which produces a scan pattern with 5 parallel scan lines (2 forward, 1 nadir, 2 backward) to have a large coverage even in narrow and complex environments. The scan lines have different incidence angles with varying scan directions along tracks (Figure 3). The across track field of view is ca ± 30 deg. The clear advantage of scanning with different angles, especially in urban contexts, is to increase the coverage on vertical structures, small courtyards and narrow streets.

3. Data, Experiments and Analyses

The dataset used in our analyses was acquired over the city of Graz (Austria) in June 2024, at a flight altitude of 1060 m with an overlap of 80% forward and 60% sideward. Considering these flight parameters and the 45 deg inclination of oblique cameras, nadir images overlap with oblique views acquired in strips ca 1 km away (Figure 1-below). The dataset counts a total of 334 oblique and nadir images (5 cm GSD) over the city center, LiDAR data (~250 million points), GNSS-based trajectory observations and 13 GNSS-surveyed ground control points distributed within the area. The eight LiDAR strips covering the area of interest (AOI) of about 3.5 km^2 were adjusted and merged with the Riegl software.

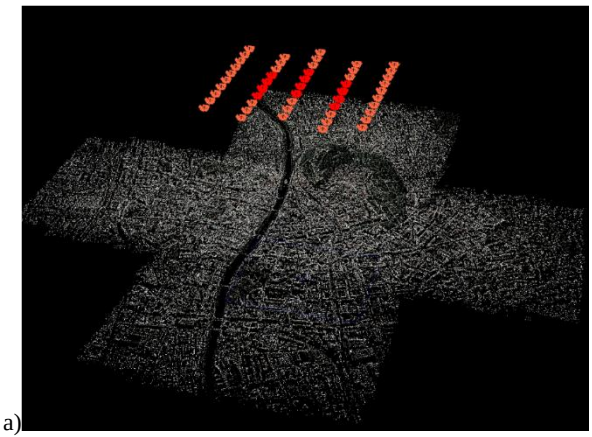
a)

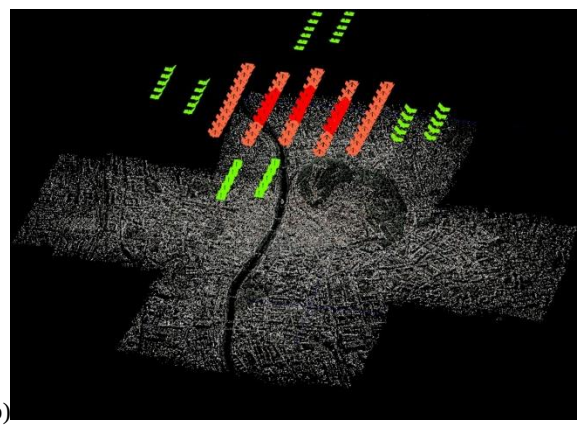
b)

Figure 4. The two image blocks: 5 strips with 250 cameras (a); 334 cameras (b), with the inclusion of further nadir and oblique images highlighted in green. In red the cameras used for the connectivity analysis.

Two sub-blocks are considered (Figure 4): the first with a subset of the imagery covering an area of approximately 1 km^2 and including 5 strips with 250 aerial images (Figure 4a) and a second dataset which integrates additional 84 nadir and oblique cameras in lateral and longer strips (Figure 4b). The aim is to show how oblique image blocks need many more strips and images with respect to nadir-only blocks to fully exploit the intrinsic advantages of the slanted views.

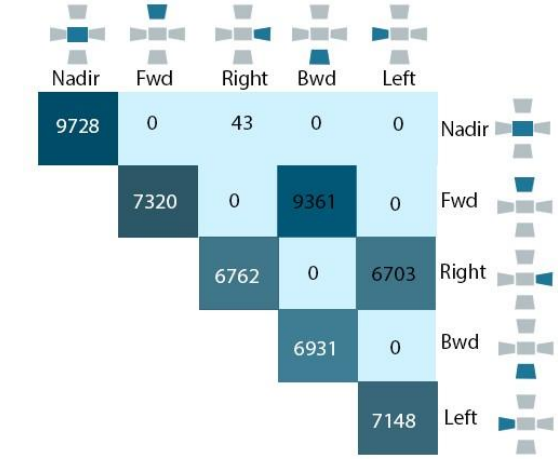

a)

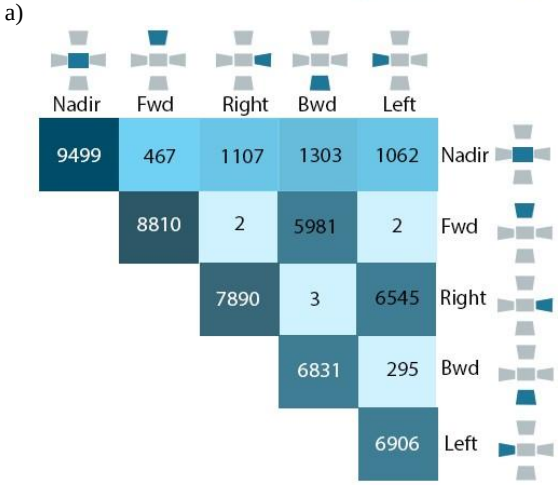

b)

Figure 5. Image connectivity between nadir and oblique views. In an image block with few strips (a – Figure 4a) no or few correspondences are found between the slanted view. Considering more strips (b), the number of tie points increases.

3.1 Connectivity Analysis With Hand-Crafted Image Matching Features

Automatic tie point matching involving oblique cameras remains highly challenging due to geometric distortions, perspective variations and reduced overlap between different views affecting tie point extraction and matching techniques. Common AT methods involve SIFT-like methods for the extraction of image correspondences. Using the two image blocks shown in Figure 4, an image connectivity analysis is performed considering the 60 images in the 3 central strips. The evaluation focuses on the number of correspondences founded among different camera views. The matching results presented in Figure 5 show that oblique views from external strips must be included in order to better tie nadir and slanted views. With just a small number of strips, nadir images have no (or very few) tie points with oblique views (Figure 5a) whereas a larger block with more strips allows to find more correspondences among all views (Figure 5b). Nevertheless, in some cases (e.g. left-forward or rightbackward), it is still a challenge to find a sufficient number of well distributed tie points, even with a larger dataset. This limitation of hand-crafted methods could be improved with deep learning methods.

3.2 Deep Learning-Based Image Matching

In recent years, new matching methods based on convolutional neural networks and graph neural networks have been introduced and trained on large datasets to address the limitations of traditional approaches, such as SIFT (Lowe, 2004). Their two primary advantages include strong invariance to illumination changes - particularly beneficial for multi-temporal datasets and robustness in matching images with substantial geometric distortions, e.g. as nadir-to-oblique or oblique-to-oblique aerial images. Following initial analyses presented in Remondino et al. (2022) and using the Deep-Image-Matching tool - DIM[1] (Morelli et al., 2024), SuperPoint (DeTone et al., 2018) and LightGlue (Lindenberger et al., 2023) were selected and tested on five challenging pairs of nadir-oblique and oblique-oblique images to evaluate the effectiveness of these new matchers. The extracted tie points were compared with those obtained using SIFT, followed by exhaustive nearest-neighbor matching and geometric verification with DEGENSAC (Chum et al., 2005). Results are reported in Figure 6, where blue dots and green lines indicate correct tie points. The graphical and numerical comparisons show that learning-based methods can in general find more correspondences and ensure greater redundancy of observations. In a right-backward pair (Figure 5) no correspondences could be found at full image resolution. Reducing the image resolution in DIM from high (14144 x 10560 px) to low (3536 x 2640 px) and lowest (1768 x 1320 px), it becomes possible to extract matches using SuperPoint + LightGlue. In contrast, SIFT fails to extract matches at any resolution. While this result underlines the robustness and potential of SuperPoint, it also reveals a degree of scale dependency in its performance. Since the tie points are extracted at low resolution, a refinement of the keypoints by extracting patches from the high-resolution images would be necessary to achieve greater accuracy.

3.3 Aerial Triangulation

Different processing approaches are applied to the entire image block (334 images) to investigate the quality of the Aerial Triangulation (AT). In particular:

- Direct georeferencing (Mostafa and Hutton, 2001; Skaloud, 2002) through positional data derived from GNSS receivers embedded in the hybrid system, with exterior orientation parameters derived from the refined trajectory and knowing the relative orientation between nadir and oblique images.
- Bundle Block Adjustment (BBA), including GNSS-surveyed control points (6 GPCs and 7 CPs) with a mean 3D accuracy of 3 cm.
- BBA using control points measured in the concurrently acquired LiDAR point cloud (6 GCPs and 7 CPs). These points were manually identified in the point cloud in the same areas of the GNSS-surveyed points.

[1] https://github.com/3DOM-FBK/deep-image-matching

Figure 6. Matching results with a hand-crafted (SIFT) and a learning-based (SuperPoint + LightGlue) methods. Keypoints are extracted and matched at full image size (14144 x 10560 px) using the DIM tiling strategy.

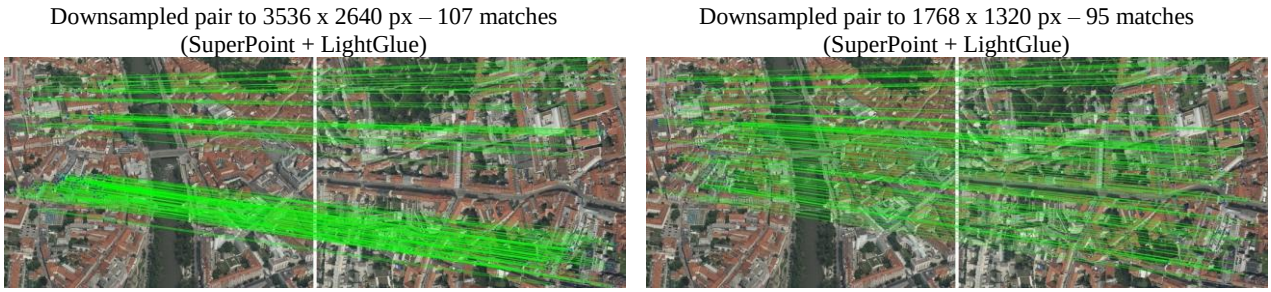

Figure 7. Image pair (right-backward) where no tie points could be extracted at full resolution but only downsampling the images.

		Direct georeferencing		BBA with GNSS points		BBA with LiDAR points	
		RMS [cm]	Max [cm]	RMS [cm]	Max [cm]	RMS [cm]	Max [cm]
GCPs	X	-	-	1.489	1.657	7.498	12.198
	Y	-	-	0.407	0.422	9.823	17.788
	Z	-	-	1.306	2.363	2.971	4.369
CPs	X	16.401	28.692	1.782	2.968	4.711	7.320
	Y	17.056	28.152	4.867	12.58	11.754	20.589
	Z	38.401	55.310	3.841	6.452	7.510	13.467

Table 1. Metrics of the three different processes: direct georeferencing, BBA with 6 GNSS-based GCPs and BBA with 6 LiDARbased GCPs. The GSD of nadir images is 5 cm.

In all cases, the interior parameters (IO) of all cameras were not estimated but kept fixed based on the calibration certificate. The statistics of the AT for all three cases are reported in Table 1. Direct georeferencing proved to be a viable option only for specific applications, such as rapid mapping (Toschi et al., 2017b). The AT results based on GNSS-surveyed control points show accuracy values within 1 GSD. When LiDAR-based control points are included as constraint, 2x larger errors are observed on the check points. In this case, accuracy values are mainly affected and conditioned by the complexity of correctly measuring points in the LiDAR point cloud and corresponding imaging dataset.

3.4 Evaluation of Data Integration on 3D Reconstruction

The quality of the 3D reconstruction derived from the hybrid concurrent aerial acquisition is assessed with quantitative and qualitative analyses. The evaluation is performed by comparing the outputs of the photogrammetric dense image matching based on the MSP semi-global matching algorithm[2], LiDAR data and integration results. Specifically, the following scenarios are examined:

1) photogrammetric dense image matching leveraging only nadir images;
2) photogrammetric dense image matching utilizing the entire nadir and oblique dataset (334 cameras);
3) LiDAR data;
4) integration of the full imaging dataset (nadir and oblique) and LiDAR data, assuming correct georeferencing of the data.

For the quantitative evaluation, the point density (pts/m^2) of different reconstructions is compared by extracting about 30 patches well distributed in the city for each of the categories listed in Table 2 and shown in Figure 8. These patches isolate urban elements with varying levels of occlusions.

Furthermore, the advantage of imaging and LiDAR data integration is examined extracting profiles in several areas, including both urban and vegetated parts (Figure 9):

1) A-A' profile: a densely urbanized area characterized by narrow spaces between adjacent buildings and several internal courtyards. This area poses challenges associated with complex geometries and shadowed regions.
2) B-B' profile: a mostly vegetated region, including lawn and wooded areas. The profile is selected to assess the reconstruction capabilities under vegetation cover.
3) C-C' profile: it includes buildings with less collaborative surfaces for photogrammetric applications (a glazed building) and some vegetated areas. This area represents a typical scenario where photogrammetric approaches face difficulties due to poor texture or surface properties.

Point cloud density (Table 2), profiles (Figure 9) ad close-ups (Figure 10) show that the integration's gain is especially relevant to enhancing the photogrammetric results in partially occluded areas and low-texture surfaces. Integrating imaging and ranging technologies enables a more robust reconstruction process that is adaptable to various urban and natural environments, beside supporting terrain modelling and addressing the traditional limitations of photogrammetric techniques

Figure 8. Examples of patches (colored regions) identified to compute the point cloud density.

3.5 The MEASUREE Tool

The processed aerial (nadir & oblique) block can be visualized and inspected through the powerful web-based tool MEASUREE[3] developed by AVT Airborne Sensing (Figure 11). It stems from the former Geobly tool - GEOmetry extraction tool from aerial OBLique imagery (Moe et al., 2016; Poli et al., 2017) and it offers a high-powered online solution to manage large nadir and oblique datasets. Thanks to the web-based implementation, users only need a conventional web browser to start working with the oriented vertical and oblique images of a flight. It also does not require any special and often expensive hardware, as is typically required in "classic" photogrammetry (synchronous stereoscopic measurement). One of the major challenges with multi-perspective flights is the very large amount of data and the generally confusing nature of oblique datasets. MEASUREE addresses this problem through effective image compression, tiling and image pyramid formation as well as very elegant sorting methods (e.g. according to spatial proximity). In this way, users are almost completely relieved of the timeconsuming task of searching for the images most suitable for a task.

MEASUREE measurement methods rely on the oriented aerial images and can be performed on single (monoplotting) or multiple images. Simple measurements such as distances, lengths, height differences or surface areas can be quickly and easily carried out by inexperienced users. But MEASUREE also offers experts a wealth of options for highly accurate and reliable mapping and 3D modeling of complex objects and scenes, as well as for quality assurance of 3D data sets.

For images containing sensitive data, such as military facilities, the tool includes an automated declassification module able to generate new images from the original ones, where these objects are removed or made unrecognizable (for example, using pixelization or blurring effects).

MEASUREE can also be used to manage data coming from different flight platforms (aircraft and drone) and sensor systems (nadir, oblique, thermal infrared, hyperspectral).

Scenario	Category	Nadir		Nadir+Obliques		LiDAR		Integrated	
		Mean	*St. Dev.*	*Mean*	*St. Dev.*	*Mean*	*St. Dev.*	*Mean*	*St. Dev.*
Open areas	Streets	64.35	13.64	73.30	14.66	74.99	17.51	158.45	36.59
	Roofs	89.16	16.16	103.95	19.46	63.45	15.21	175.62	37.83
Partially occluded areas	Facades	58.80	22.84	103.85	27.92	15.76	9.00	114.95	36.10
	Vegetation	82.53	25.36	97.08	30.13	47.29	24.38	132.38	51.76

Table 2. Point cloud density (pts/m^2) for the different scenarios, evaluated on ca 30 well distributed patches for each category.

[2] https://u.osu.edu/qin.324/msp

[3] https://measuree.net/index_en.html?lang=en

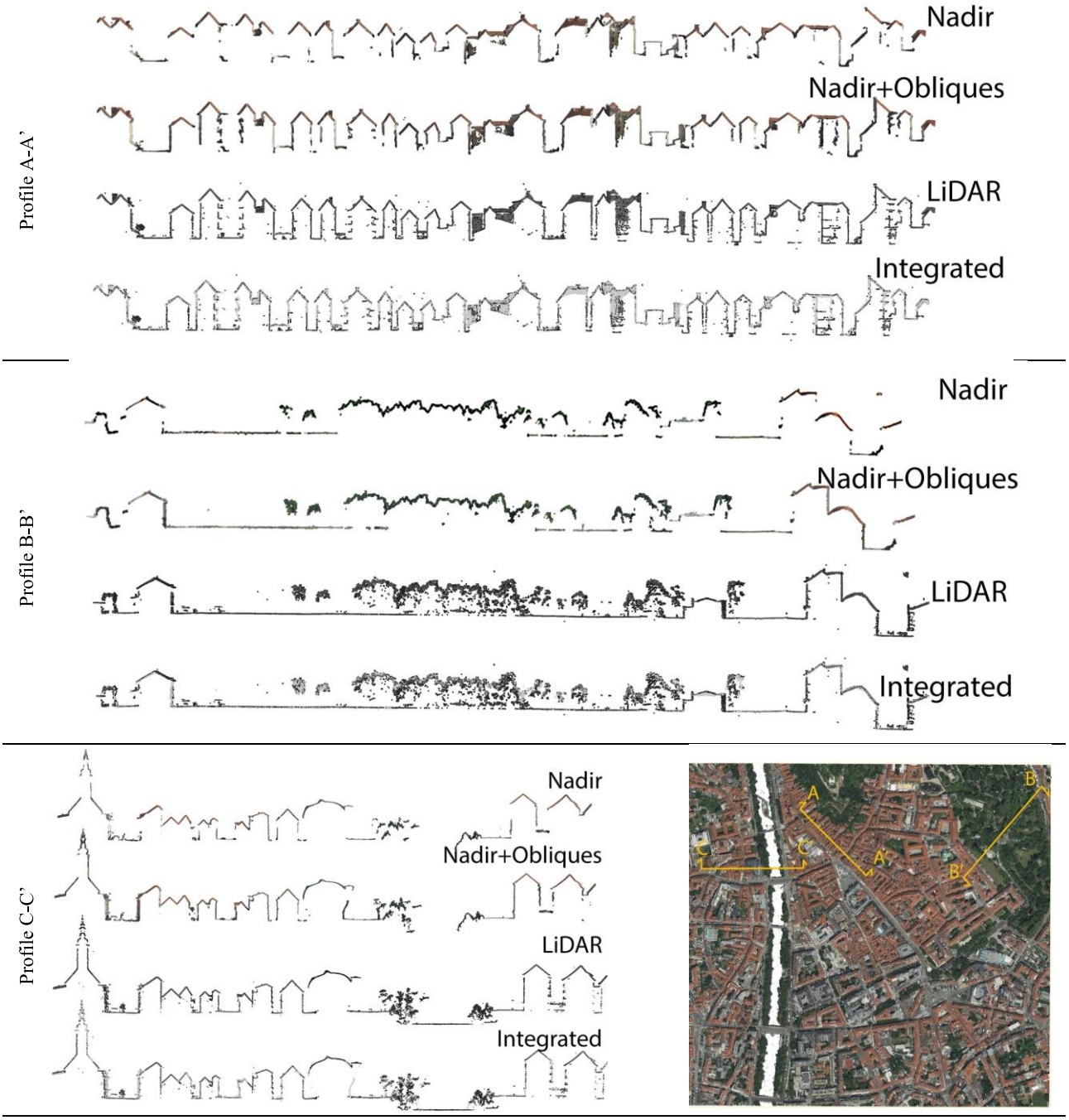

Figure 9. Extracted profiles for qualitative analyses of the 3D reconstruction and integration processes.

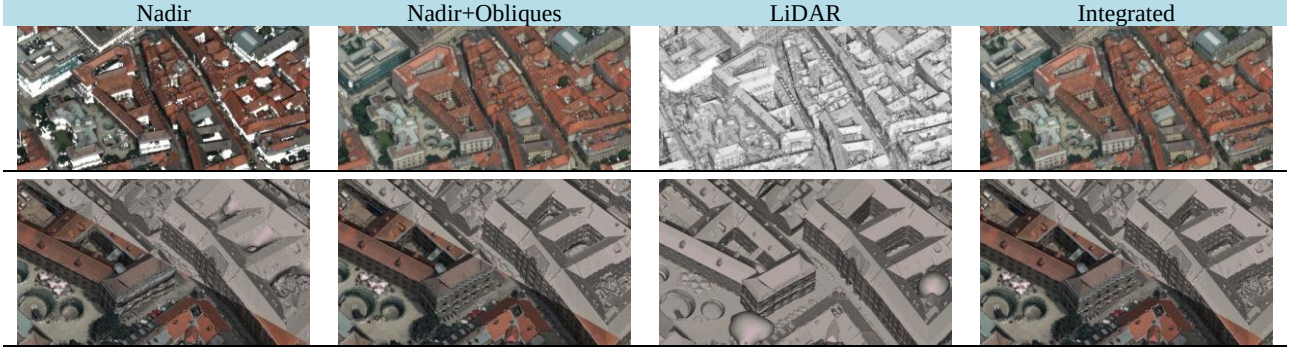

Figure 10. Close views to the dense point clouds (top) and generated mesh models (below) – Poisson algorithm.

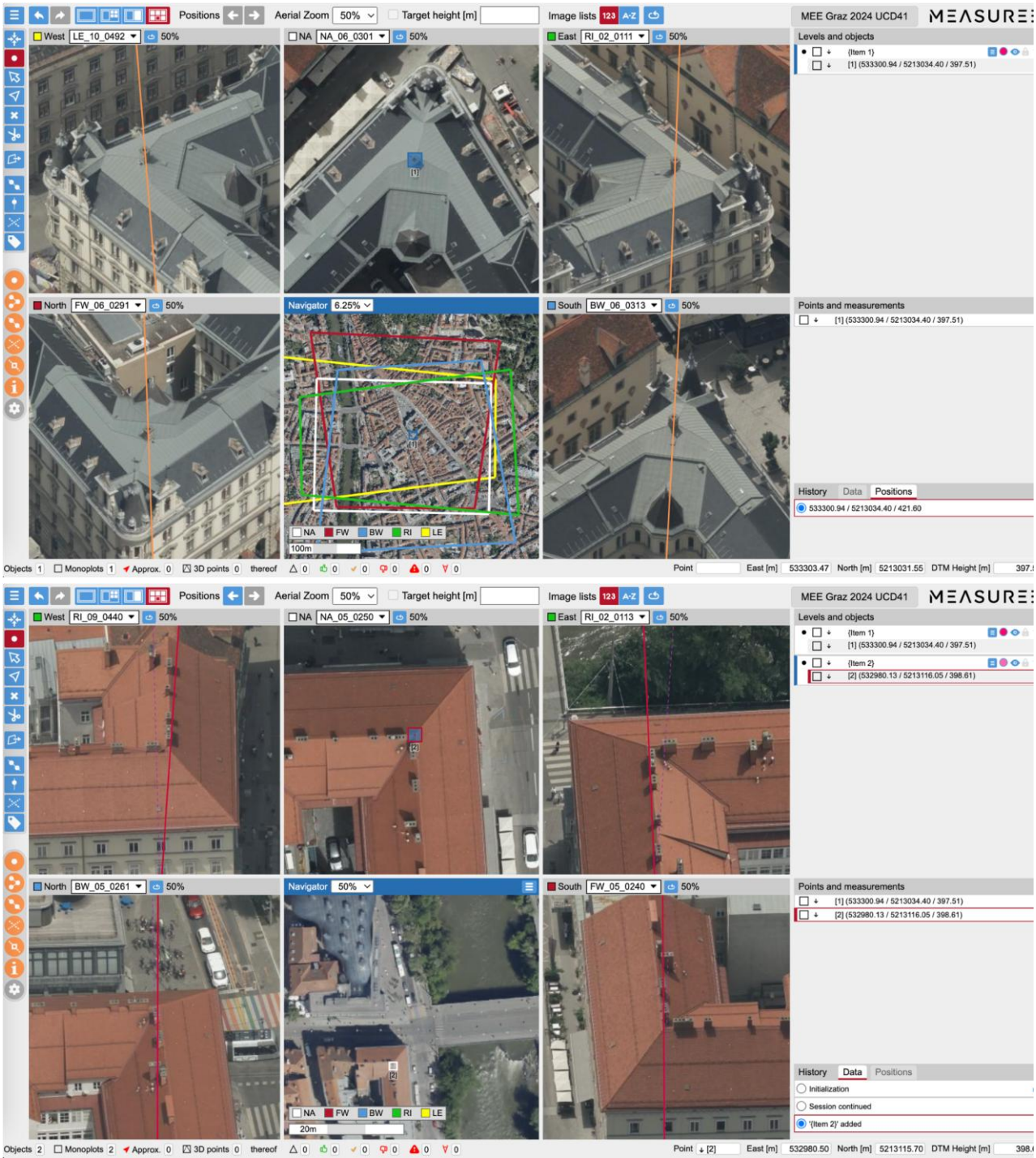

Figure 11. Views of the web-based MEASUREE photogrammetric tool for measurement and inspection of large oblique blocks.

4. Conclusions

The paper reported a first investigation of the ULTRACAM DRAGON 4.1, the new hybrid airborne system offered by Vexcel Imaging. The analysis of AT and 3D reconstruction results showed the advantages of combining imaging and ranging data, ideally into a unified framework, by exploiting their complementary strengths and overcome respective traditional limitations. The hybrid system can leverage the benefits of LiDAR sensing with superior height accuracy and vegetation penetration capabilities while exploiting enhanced radiometric properties and higher 3D point density from the multi-camera imaging system. The concurrent acquisition of data avoids temporal discrepancies and changes in the acquired dataset, facilitating seamless data fusion. GCPs from the LiDAR point cloud could also support the AT process.

Nevertheless, hybrid solutions are nowadays calling the design of a truly integrated and automated processing workflow to unlock the full potential of combined sensors. Such integrated processing could minimize inconsistent data registration, speed up processing, improve dense point clouds or mesh models. The processing could exploit emerging learning-based algorithms for image matching, which are particularly helpful when processing different perspective views.

References

Bacher, U., 2021. 3D Content Generation using Hybrid Aerial Sensor Data. *Int. Arch. Photogramm. Remote Sens. Spatial Inf. Sci.*, 43, 297303.

Bacher, U., 2022. Hybrid aerial sensor data as basis for a geospatial digital twin. *Int. Arch. Photogramm. Remote Sens. Spatial Inf. Sci*., 43, 653-659.

Cavegn, S., Haala, N., Nebiker, S., Rothermel, M., Tutzauer, P., 2014. Benchmarking high density image matching for oblique airborne imagery. *Int. Arch. Photogramm. Remote Sens. Spatial Inf. Sci*., 40, 45-52.

Chum, O., Werner, T., Matas, J., 2005. Two-view geometry estimation unaffected by a dominant plane. *Proc. CVPR*, 1, 772779.

DeTone, D., Malisiewicz, T., Rabinovich, A., 2018. Superpoint: Selfsupervised interest point detection and description. *In Proc. CVPR*, 224-236.

Fernández, T., Pérez-García, J.L., Gómez-López, J.M., Cardenal, J., Moya, F., Delgado, J., 2021. Multitemporal landslide inventory and activity analysis by means of aerial photogrammetry and LiDAR techniques in an area of Southern Spain. *Remote sensing*, 13(11), 2110.

Glira, P., Pfeifer, N., Mandlburger, G., 2019. Hybrid orientation of airborne lidar point clouds and aerial images. *ISPRS Ann. Photogramm. Remote Sens. Spatial Inf. Sci.*, 4, 567-574.

Huang, X., Qin, R., Xiao, C., Lu, X., 2018. Super resolution of laser range data based on image-guided fusion and dense matching. *ISPRS Journal of Photogrammetry and Remote Sensing*, 144, 105-118.

Lemmens, M., 2020. Capturing LiDAR and imagery simultaneously: How major cities may benefit from a hybrid sensor system. *GIM International*, 34, 10-13.

Lindenberger, P., Sarlin, P.E., Pollefeys, M., 2023. Lightglue: Local feature matching at light speed. *Proc. ICCV*, 17627-17638.

Lowe, D.G., 2004. Distinctive image features from scale-invariant keypoints. *Int. Journal of Computer Vision*, 60, 91-110.

Jin, Y., Mishkin, D., Mishchuk, A., Matas, J., Fua, P., Yi, K.M., Trulls, E., 2021. Image matching across wide baselines: From paper to practice. *International Journal of Computer Vision*, 129(2), 517-547.

Jonassen, V.O., Kjørsvik, N.S., Gjevestad, J.G.O., 2023. Scalable hybrid adjustment of images and LiDAR point clouds. *ISPRS Journal of Photogrammetry and Remote Sensing*, 202, 652-662.

Jonassen, V.O., Kjørsvik, N.S., Blankenberg, L.E., Gjevestad, J.G.O., 2024. Aerial hybrid adjustment of LiDAR point clouds, frame images and linear pushbroom images. *Remote Sensing*, 16(17), 3179.

Kocaman, S., Akca, D., Poli, D., Remondino, F., 2022. *3D/4D City Modelling - From Sensors to Applications*. Whittles Publishing, ISBN: 978-184995-475-4, 224 pages.

Mandlburger, G., Wenzel, K., Spitzer, A., Haala, N., Glira, P., Pfeifer, N., 2017. Improved topographic models via concurrent airborne LiDAR and dense image matching. *ISPRS Ann. Photogramm. Remote Sens. Spatial Inf. Sci.*, IV-2/W4, 259-266.

Megahed, Y., Shaker, A., Yan, W.Y., 2021. Fusion of airborne LiDAR point clouds and aerial images for heterogeneous land-use urban mapping. *Remote Sensing*, 13(4).

Moe, K., Toschi, I., Poli, D., Lago, F., Schreiner, C., Legat, K., Remondino, F., 2016. Changing the production pipeline - use of oblique aerial cameras for mapping purposes. *Int. Arch. Photogramm. Remote Sens. Spatial Inf. Sci*., 41-B4, 631-637.

Morelli, L., Ioli, F., Maiwald, F., Mazzacca, G., Menna, F., Remondino, F., 2024. Deep-image-matching: a toolbox for multiview image matching of complex scenarios. *Int. Arch. Photogramm. Remote Sens. Spatial Inf. Sci*., 48, 309-316.

Mostafa, M.M.R., Hutton, J., 2001. Direct Positioning and Orientation Systems: How Do They Work? What is The Attainable Accuracy? Proc. *ASPRS Annual Meeting*, St. Louis, MO, USA.

Norton, C.L., Hartfield, K., Collins, C.D.H., van Leeuwen, W.J., Metz, L.J., 2022. Multi-temporal LiDAR and hyperspectral data fusion for classification of semi-arid woody cover species. *Remote Sensing*, 14(12), 2896.

Poli, D., Moe, K., Legat, K., Toschi, I., Lago, F., Remondino, F., 2017. Use of vertical aerial images for semi-oblique mapping. *Int. Arch. Photogramm. Remote Sens. Spatial Inf. Sci*., XLII-1-W1, 493-498.

Remondino, F., Gerke, M., 2015. Oblique aerial imagery– a review. *Proc. Photogrammetric Week*, 15(12), 75-81.

Remondino, F., Toschi, I., Gerke, M., Nex, F., Holland, D., McGill, A., Talaya Lopez, J., Magarinos, A., 2016. Oblique aerial imagery for NMA - Some best practices. *Int. Arch. Photogramm. Remote Sens. Spatial Inf. Sci*., 41-B4, 639-645.

Remondino, F., Morelli, L., Stathopoulou, E., Elhashash, M., Qin, R., 2022. Aerial triangulation with learning-based tie points. *Int. Arch. Photogramm. Remote Sens. Spatial Inf. Sci*., 43, 77-84.

Rupnik, E., Nex, F., Toschi, I., Remondino, F., 2015. Aerial multicamera systems: Accuracy and block triangulation issues. *ISPRS Journal of Photogrammetry and Remote Sensing*, 101, 233-246.

Skaloud, J., 2002. Direct georeferencing in aerial photogrammetric mapping. *Photogrammetric Engineering & Remote Sensing (PERS)*, 68(3), 207-210

Toschi, I., Ramos, M.M., Nocerino, E., Menna, F., Remondino, F., Moe, K., Poli, D., Legat, K., Fassi, F., 2017a. Oblique photogrammetry supporting 3D urban reconstruction of complex scenarios. *Int. Arch. Photogramm. Remote Sens. Spatial Inf. Sci*., 42, 519-526.

Toschi, I., Remondino, F., Kellenberger, T., Streilein, A., 2017b. A survey of geomatics solutions for the rapid mapping of natural hazards. *Photogrammetric Engineering & Remote Sensing (PERS)*, 83(12), 843-860.

Toschi, I., Remondino, F., Rothe, R., Klimek, K., 2018. Combining airborne oblique camera and LiDAR sensors: Investigation and new perspectives. *Int. Arch. Photogramm. Remote Sens. Spatial Inf. Sci*., 42, 437-444.

Toschi, I., Remondino, F., Hauck, T., Wenzel, K., 2019. When photogrammetry meets LiDAR: Towards the airborne hybrid era. *GIM International*, Sept issue, 17-21.

Toschi, I., Farella, E.M., Welponer, M., Remondino, F., 2021. Quality-based registration refinement of airborne LiDAR and photogrammetric point clouds. *ISPRS Journal of Photogrammetry and Remote Sensing*, 172, 160-170.

Yadav, Y., Alsadik, B., Nex, F., Remondino, F., Glira, P., 2023. Hybrid adjustment of UAS-based LiDAR and image data. *Int. Arch. Photogramm. Remote Sens. Spatial Inf. Sci*., XLVIII-1/W2-2023, 633-640.